

# Evaluation of the Silicon on Glass Microfabrication Process for MEMS Accelerometers

Thomas S. White  
Central Michigan University  
[white1ts@cmich.edu](mailto:white1ts@cmich.edu)

Kevin Petsch  
Central Michigan University  
[petsc1k@cmich.edu](mailto:petsc1k@cmich.edu)

Tolga Kaya  
Central Michigan University  
[kaya2t@cmich.edu](mailto:kaya2t@cmich.edu)

## Abstract

We present a testing procedure and the results of a capacitive triaxial accelerometer intended for health and safety applications. Static and quasi-static tests were performed to gain insight into the overall functionality of devices and the effectiveness of the silicon on glass (SOG) microfabrication process performed at the Lurie Nanofabrication Facility of the University of Michigan, Ann Arbor. SOG was incorporated into the design to reduce parasitic capacitances because they can impede accuracy and sensitivity. Understanding how this form of wafer bonding impacts the design is key to understanding the capabilities of the accelerometers. Capacitance reading yields showed ranges within predicted limits and deviations caused by the fabrication process. The highest change in capacitance was 94.1% during quasi-static tests, while the lowest change was 7.6%. Out of 1259 devices tested on a 4'' wafer, 34 of them passed, yielding a 2.7% success. Our simple process elimination method lets accelerometer tests less time consuming and makes the process optimization viable.

## Introduction

The field of MEMS (microelectromechanical systems) technological research continuously expands. Applications can be found in numerous technologies such as smartphones, laptop computers, inkjet printers, microphones, and micro-scale lasers [1-7]. Factors that make MEMS devices so attractive include their relative reliability, low cost, and ability to be mass-fabricated [8]. In particular, MEMS-based accelerometers appear to have many possible applications [9-16]. In civil engineering, capacitive accelerometers have shown promise for gauging strain placed upon bridges through integration into sensing and transmission systems [15]. Companies such as BP and Shell have found capacitive accelerometers offer benefits of lower-power consumption, reduced signal noise, and wider device dispersion for exploring oil and gas deposits [9]. Medical institutions explore possible applications for these sensors in areas such as monitoring heart bypass patients and collecting data relating to gait and balance in the elderly [16, 17]. For individuals at a higher risk of falling, like the elderly and disabled, low-G (up to 4 G) motion sensors have the potential to increase personal safety

through monitoring physical activity [16, 17]. Emergency response personnel can be notified immediately when the motion sensors register a falling event and signal to quickly bring assistance.

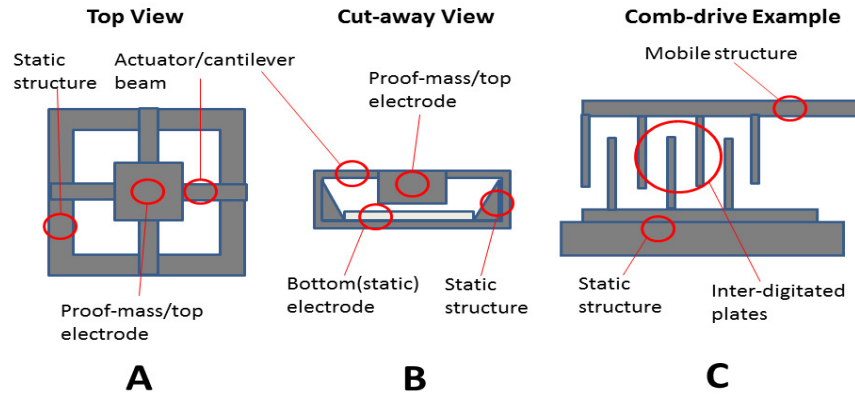


Figure 1. Examples of an accelerometer: A) from the top and B) from the side cut-away view. C) An example of a simple comb-drive

Capacitive accelerometers measure capacitance changes between a mobile electrode (the proof-mass in this case) and bottom electrode (Figure 1a and 1b) [6, 10, 17]. Capacitive accelerometers often depend on actuators such as cantilever beams, spring structures or folded flexures to support a central proof-mass and allow it move as depicted in Figure 1a [6, 10, 17, 28]. Capacitance ( $C$ ) values can be calculated as

$$C = \frac{\epsilon A}{d} \quad (1)$$

$A$  represents the area of the capacitance plates and  $\epsilon$  denotes the permittivity of the dielectric material (between the plates). Lastly,  $d$  symbolizes the distance between the capacitance plates. A change in capacitance corresponds to changes in displacement of the proof-mass [6, 10, 17-20]. The distance between the plates and the resulting capacitance values have an inverse relationship. Another accelerometer design incorporates a comb-drive consisting of interdigitated electrodes that form parallel-capacitance plates as shown in Figure 1c [6, 11, 17]. The type of accelerometer incorporated into a sensing system is determined by the needs of system designers. The capacitive signals generated by such sensors are relayed through a digital converter and sent to a computer or a recording device so that data can be analyzed [4, 15, 17, 21].

The accelerometer design discussed in this paper is intended for health and safety monitoring. It incorporates both comb-drives and a mobile proof-mass/bottom electrode mechanism in the same device (see Figure 2a). The comb-drive measures capacitance along the x-, and y- planes as illustrated in Figure 2b [11, 17]. Tilt and z- directional readings are accommodated by the proof-mass and bottom electrode. The flexible spring structures (see Figure 2c) actuate the proof-mass and allow not only a 3-dimensional range of motion, but also a high sensitivity [11]. This type of motion sensor could eventually integrate piezoelectric materials that could help make them energy efficient as well as more accurate [22, 23].

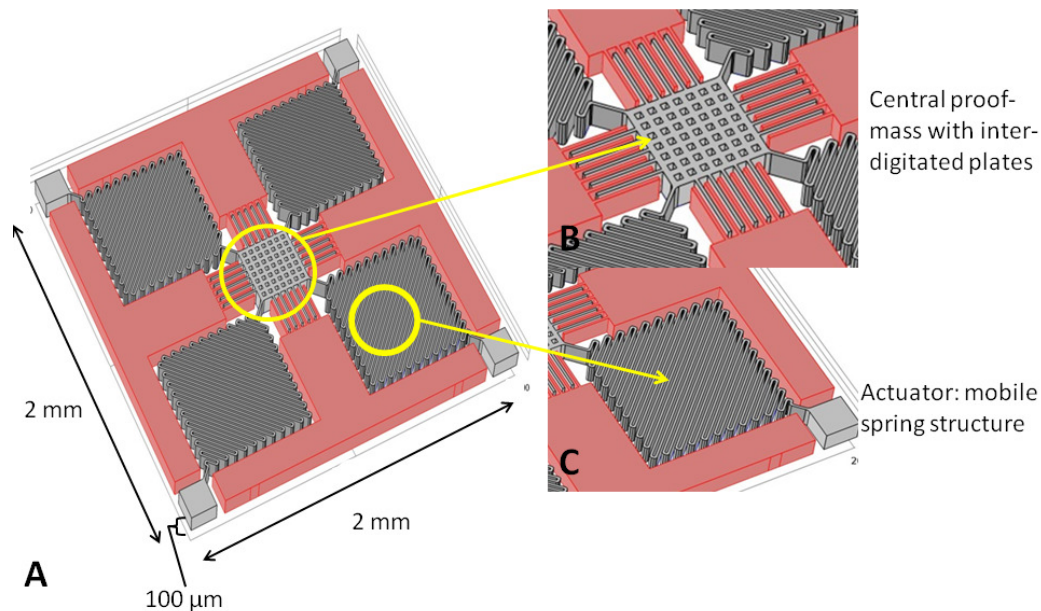


Figure 2. A) Comb-drive accelerometer designed to function along the x-, y-, and z- planes. B) Proof-mass with interdigitated, parallel capacitance plates. C) The flexible spring structure that enables the mobility of this design. The entire package is 2 mm × 2 mm × 100 μm. The red regions are immobile and the grey regions are mobile.

The sensitivity of the device depends strongly on the proper fabrication and material selection procedures. It was decided that silicon and glass wafers together would perform best in this case. SOG anodic bonding was used to bond silicon and glass wafers together by applying an electric potential across both wafers [24 & 25]. A major benefit of SOG is that the glass' non-conductive nature helps reduce parasitic capacitances that could reduce the accuracy and overall effectiveness of the sensors [17].

Testing can be static, quasi-static, and dynamic in nature. Static tests require no movement of any mobile structures. An example of a static test that we conducted involved checking the resistance along a stationary electrode to verify its function. Quasi-static examinations allowed the electrical and mechanical performance of a device to be checked in a single direction at a time. For example, we moved the proof-mass to the left (the negative x-direction in this case) to measure the change in capacitance. Static and quasi-static evaluations were initially performed because they gave a direct and fast result of a device's functionality. Devices that passed these tests are good candidates for later dynamic testing. Dynamic tests allow the full range of an accelerometer's motion and sensitivity to be observed by a method like a shaker or Electron Speckle Pattern Interferometry [1, 6, 10, 26-28]. They are a means to evaluate a sensor's performance in an environment that more closely simulates real-life conditions. But before this can happen, the design and fabrication processes need to be evaluated. We want to understand the reliability of the SOG process. Therefore, we tried different designs to see the yield. Yield analysis and percent evaluations,

based upon the gathered data offered a clear picture of how the devices actually performed in terms of consistency and reliability. We will discuss our fabrication process, static tests conducted, different design variations, and failed devices. Dynamic tests were not performed and will be discussed in a later paper.

### Design and Fabrication

The development of the particular designs discussed here incorporated computer drafting and finite element analysis simulations via COMSOL Multiphysics. Fabrication occurred at the University of Michigan's Lurie Nanofabrication Facility and the specific details of fabrication are explained in a previous work [17]. Fabrication of the devices included standard MEMS techniques such as photolithography, metal deposition, hydrofluoric acid etching of the glass substrate, anodic bonding of the glass and silicon wafers, and dry etching for shaping and releasing each device's mobile structures [17]. The silicon wafers are 0.1mm thick and the glass wafer is 0.5mm thick producing a combined wafer of 0.6 mm in thickness [17]. Temperature is controlled during the fabrication process in each step so as not to allow high diffusion-temperature time to degrade the device performance. The finished product of fabrication is a wafer containing nearly 1,200 devices. The devices are organized into  $5 \times 5$  geometric groups called dies. A die consists of 25 devices of differing dimensions and directions of functionality that is illustrated in Figure 3.

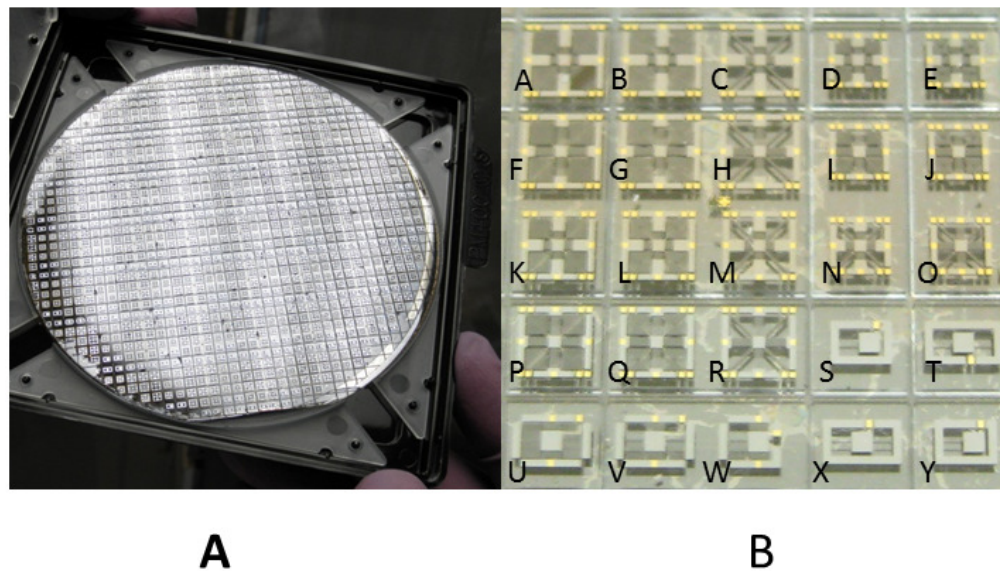


Figure 3. A) On the left is a wafer full of devices. B) Shows a die full of devices of various designs

Table 1. Devices by range and spring structure

Design Type	Sensing Range	Spring Type
A, D, F, I, K, P	3-D	Serpentine
B, E, G, J, L, Q	3-D	Spiral
C, H, M, N, O, R	3-D	Semi-serpentine
S, T, X, Y	1-D	Straight
U, V, W	2-D	Serpentine

Figure 3a shows the fabricated wafer. A full die of 25 different designs that were fabricated and tested can be seen in Figure 3b. A few representative close-look pictures are in Figure 3c. Table 1 lists devices organized by type, sensitivity and the spring actuator they employ. Accelerometers A-R function three dimensionally. Devices U-W were designed for sensing motion along the x- and z- planes. Designs S, T, X, and Y are meant to take readings in the z-direction only. The wafer contains approximately 45 complete dies of devices.

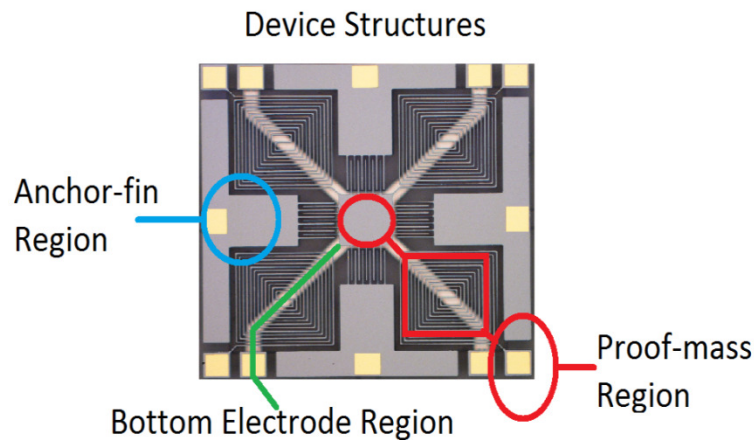


Figure 4. The various regions tested for resistance and capacitance.

Figure 4 is intended to serve as guide while different aspects of the testing process are explained. Specific regions of devices—static and mobile—are labeled clearly. Only the proof-mass is mobile. The bottom electrode and anchor-fins are static. The following descriptions for both short and capacitance testing shall refer to Figure 4.

The effectiveness of a device is examined through testing. Through proper evaluations, desired characteristics such as correct release of mobile structures, functional ability to take readings and accuracy of those readings can be verified [1, 3, 6, 17]. Devices that pass all phases of testing are considered to be successful in terms of yield.

## Testing Procedures

The testing was carried out in a soft-walled cleanroom via the Cascade Micromesh M-150 probe station as shown in Figure 5a. The set-up included a Dell desktop computer, Keithley 179-A True RMS digital multimeter (Figure 5b) and a GLK Instruments 3000 capacitance meter (Figure 5c). GrabBee video software is used for image capturing. The readings taken from the capacitance and digital multimeters were stored on Microsoft Excel data sheets that corresponded to each stage of testing. Each meter was connected to the probe station (two probes for each meter) for performing electric and mechanical testing of the devices. The data were then stored in a file on the Dropbox website to facilitate communication between members of the research team.

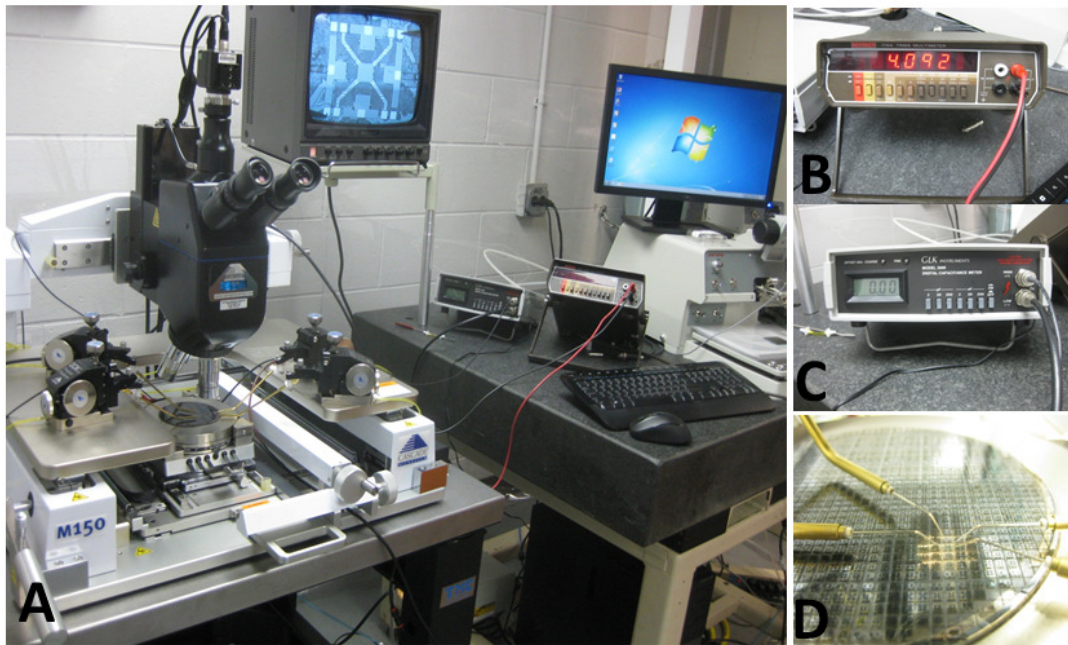


Figure 5. A) The probe and computer station where static and quasi-static tests have been performed, B) The digital multimeter, C) The capacitance meter, D) Probe tips placed on the wafer during a short test

Testing is done in a particular order. The basic reasoning is that if a device demonstrates a failure mode at a particular point of testing, then the tester can record the results and move on to another device. By process of elimination, successful devices can eventually be found in an efficient manner. Any negative capacitance reading or reading higher than the theoretical value indicates a device failure. Before static and quasi-static tests are performed, several quick inspections are done to determine if devices warrant the time required for full testing. The first thing done is a basic visual examination for any obvious damage, debris contaminants, or structural defects. If the device appears to be free of structural defects and debris contamination, the static capacitance between the proof-mass and the bottom electrode is briefly observed. The last test employs the probe tips to observe how well the proof-mass

moves and returns to its original position. Any stiction indicates a failure. Devices that pass can proceed to regular evaluations.

### Short Tests

Short testing was the first step in this process because it verified the release of mobile structures in the device. “Released” refers to the proper etching of particular structures so that they can move as intended. It also means that testing reveals no shorts between regions that are not supposed to be in contact. It should be noted that shorts can also be caused by debris such as dust contaminating a device [9]. Resistance evaluations employed a digital multimeter to check for shorting between various device regions.

When performing short tests, the only regions that should give any readings for resistance are the top electrode and the bottom electrode (see Figure 4). Both portions of the device are designed to have four contact points each. Additionally, the top and bottom electrode each act as separate closed circuits. By evaluating the resistances between their respective contact pads, it shows the functionality of each region. All other regions should show open circuits because they are separate from one another, otherwise the device fails testing. The expected readings for the proof-mass and the bottom electrode averaged  $5\text{ k}\Omega$  and  $1\text{ k}\Omega$ , respectively.

The first two regions inspected are the proof-mass and bottom electrode. The probe tips are placed at the 4 contact pads for each region denoted in Figure 4. The goal is to verify that, at least, three paths are functional along each portion distinctly. To check this, one probe tip remains stationary at a contact pad, while the other is moved between two other corresponding pads. This provides two readings that are averaged and documented. If both parts pass, then the remaining regions of the device can be examined. Resistance tests are then performed between the proof-mass and each anchor-fin section, between the bottom electrode and anchor-fins, and between the anchor-fin regions themselves, and then the proof-mass and bottom electrode. Successful devices may then move on to capacitance inspections.

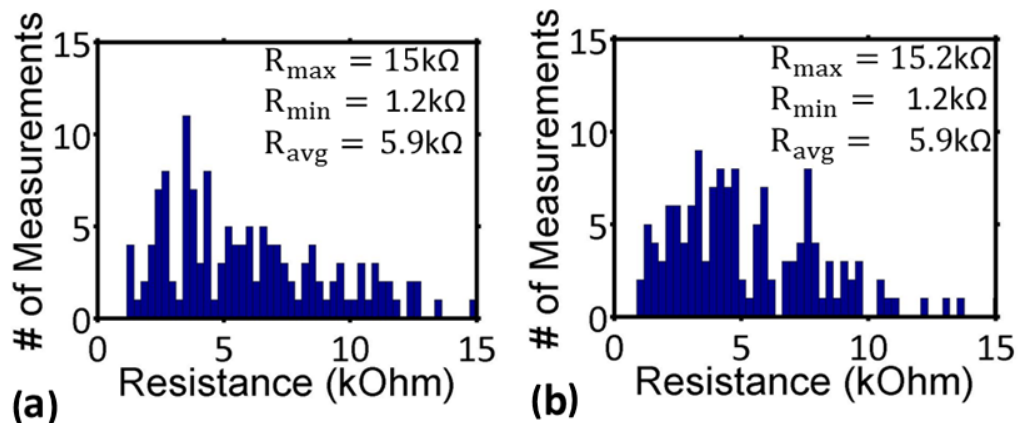


Figure 6. Resistance readings for (A) the proof-mass and (B) the bottom electrode. The highest, lowest and average values are included in the legends. A total of 129 devices were tested.

The resistance readings gathered from the proof-mass and bottom electrodes are shown in Figure 6. The values for  $R_{max}$ ,  $R_{min}$ , and  $R_{avg}$  are very close for both regions.  $R_{max}$  represents the highest resistance,  $R_{min}$  represents the lowest value, and  $R_{avg}$  is the average reading. Figure 6a demonstrates that the proof-mass had a high number of readings ranging between 3.5-4.5 k $\Omega$  —fairly close to its expected value. It also shows a trend of fewer occurrences of multiple readings within a similar range occurring as they increase in magnitude. Figure 6b shows the variations of data gathered from the bottom electrode. The data suggests that the occurrence of multiple resistances within a similar range was slightly more consistent here. It will be noted that all the resistances for the bottom electrode measured higher than its expected value of 1 k $\Omega$ . In both cases, the data shows that the resistances for both respective regions were out of their projected ranges due to fabrication process variations.

### Static Testing

Static capacitance testing followed a similar flow as resistance tests. Capacitances between the same regions were evaluated. Anything out of the acceptable range was considered a failure mode. Capacitance checks followed this order: proof-mass to anchor-fins, proof-mass to bottom electrode, and then the anchor-fin regions directly across from one another. Same as for short tests, the readings were averaged and recorded appropriately. Figure 8 helps demonstrate the sequence of this phase of evaluations.

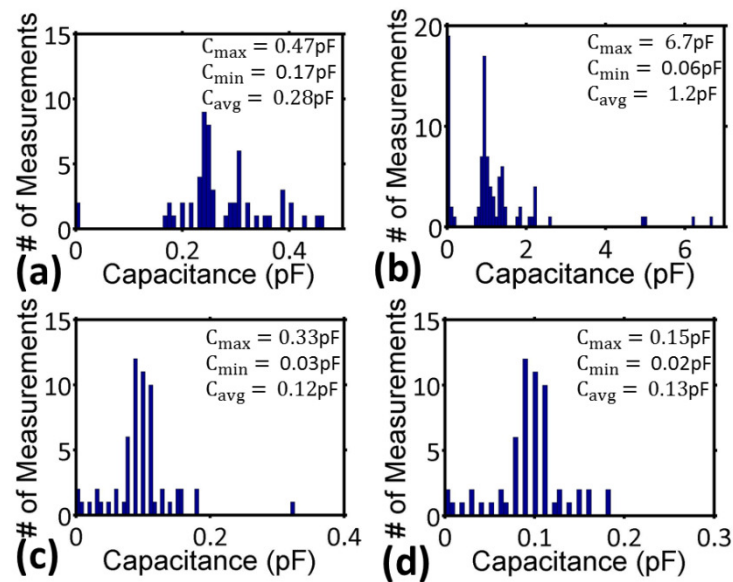


Figure 7: Capacitance readings for (A) proof-mass to anchor-fins, (B) proof-mass to bottom electrode, (C) anchor-fins horizontally across from one another and (D) anchor-fins vertically across from one another.

Results varied between the different regions testing took place.  $C_{max}$ ,  $C_{min}$ , and  $C_{avg}$  represent the highest, lowest and average capacitance readings, respectively, for each graph in Fig 7. Figure 7a demonstrates the varied data gathered while testing the devices along the x- and y-planes. The most consistent grouping of capacitances remained close to 0.23 pF. It can also be seen that readings in Figure 7a were dispersed in a relatively even fashion, starting with

the minimum value of 0.17 pF. The static performance between top electrode and bottom electrode can be seen in Figure 7b. It was the largest range between 0 pF and 7 pF. The lowest reading was 0.06 pF and the highest was 6.7 pF. Of all the locations on the device, readings here tended to rank the highest in range and frequency of approximate occurrence. This was due to the relatively large surface areas between the bottom electrode and proof-mass while they functioned as capacitance plates. The most consistently recurring readings were approximately 1 pF. The most similar sets of readings were between the anchor-fins themselves. Figure 7c and 7d show the readings for the horizontal and vertical readings. The peaks on both graphs illustrate the similar behavior in both regions. This is no surprise as all four regions are of the same basic design, yet it there is a small difference worth mentioning. Figure 9d has a higher average than Figure 7c, yet during actual testing it was observed that the average capacitance was generally 0.01 pF higher for the static capacitance plates across from one another horizontally, than for those vertically across from one another.

### *Quasi-Static Testing*

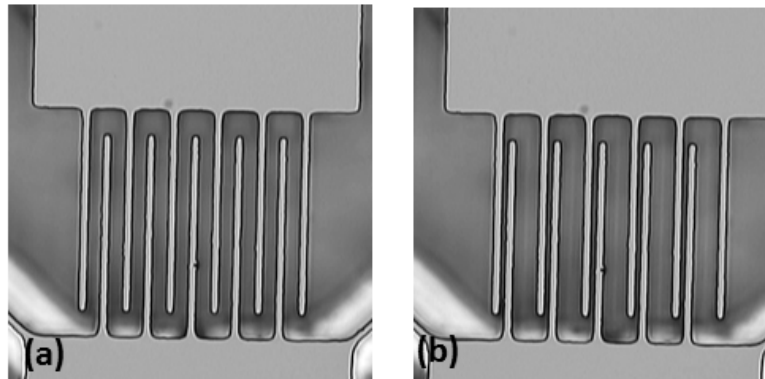


Figure 8. Optical microscopy snapshots during the quasi-static capacitance measurements. (A) Comb-drive is in stationary position. (B) Proof-mass is moved to +x- direction and the capacitance reading is recorded.

A delicate touch was needed during quasi-static tests. At the micro-scale, structures in MEMS devices can be easily damaged with a careless movement. With a small amount of practice, this method can be mastered without much difficulty. Figure 8 offers an illustration of anchor fins correctly being manipulated. It should be noticed that the fins are brought together as closely together to make note of a reading but not close enough to short them or damage the fins. Four probe tips—two stationary for measuring changes in capacitance and two to move the proof-mass—were required for this series of tests. Measurements were taken for the x- and y- directions--two sets readings each anchor-fin region (left, right, up, and down). The z-direction only provided one reading (up-down). Any readings out of range or any stiction indicated a device has failed testing. The forces exerted by the probe tips were not measured. However, it should be noted that forces in the x- and y- directions are same thanks to the symmetric design of the structure. On the other hand, the force in the z-

direction would be significantly less than the x-y plane forces because the thickness for the proof-mass and springs are only 0.1 mm whereas the x-y plane thickness is multiplied by the number and width of the beams.

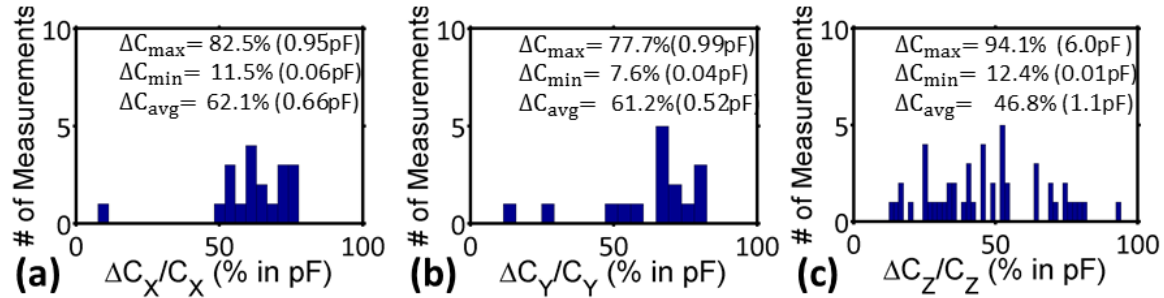


Figure 9. Capacitance change readings for the (A) x-direction, (B) y-direction, (c) z-direction

The changes in capacitance can be seen in Figure 9a-c. These charts show the percentage of capacitance change for each area of testing. Data for all three Figures were plotted to show the percentages of capacitance change in relation to the approximate number of times they came up. Also included with  $\Delta C_{max}$ ,  $\Delta C_{min}$ , and  $\Delta C_{avg}$  are the largest variations took place during z-directional examinations. The quasi-static performance for the x- and y- directional examinations revealed similar performances, but overall, the performance for the y- plane seemed to be higher than the readings of the x- axis—an average variation of 3.2% difference in performance. The performance in the x-plane revealed a slightly more consistent tendency towards repeated instances of higher percentages than the y- plane. The over-all device performance in the z-direction the most varied. It demonstrated high degrees of consistency in terms of percentage of change in capacitance—ranging between recurrences of 3 to 5 times for readings between 25 to 60 % approximately; this could be related to the varied types of devices that were designed for z-plane function.

### Device Failures and Yield Analysis

Stiction and incomplete etching most commonly caused for device failures. Figure 10 provides visual examples of some of these sources of malfunction. Both factors seemed to cause devices to fail short, capacitance, or mobility tests. Examples of these types of structural failures included anchor-fins being fused together by or to the substrate as shown in Figure 10 e and f. In some instances, the proof-mass was rendered completely immobile due to this type of fusion (see Figure 10e). A common stiction-related problem occurred when either the proof-mass would not return to its original position or a higher capacitance reading would be shown after being flexed and returned to its static position. In some instances, capacitance would actually decrease when capacitance plates were brought together. Most commonly, this seemed to happen in z- directional devices.

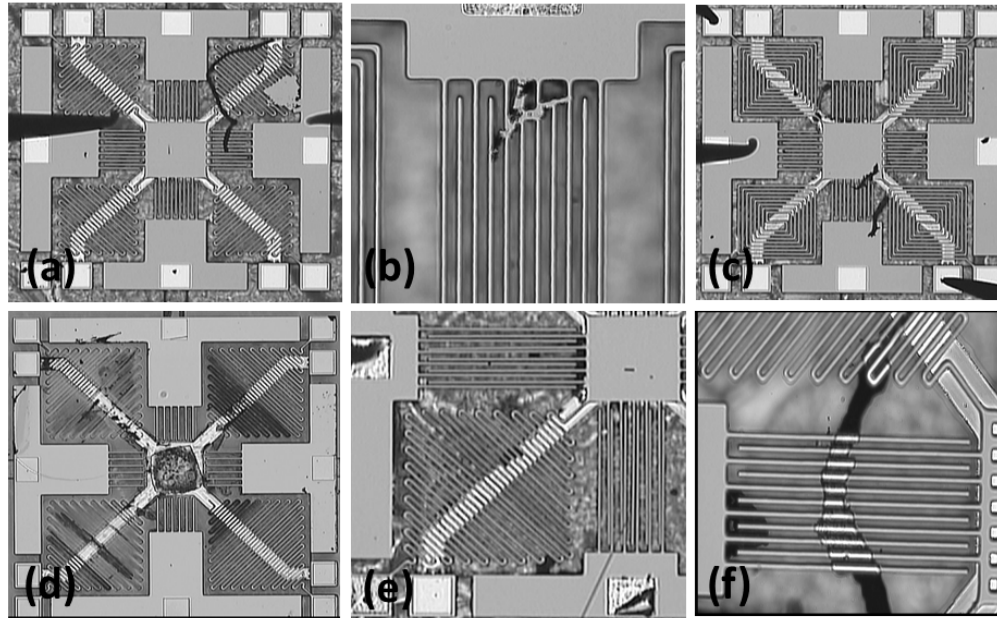


Figure 10. Various devices failures for (A) structural damage and debris contamination, (B) incomplete etching causing a short, (C) adhesion and debris, (D) destruction during fabrication, (E) stiction, and (F) adhesions from incomplete removal of the photoresist.

Table 2. Devices and percent yields from tests

	<b>Fabricated</b>	<b>Visual Exam</b>	<b>Short Tests</b>	<b>Static Tests</b>	<b>Quasi-Static Tests</b>
<b># Devices</b>	1259	819	129	98	34
<b>Yield(%)</b>	Not Applicable	65	10.2	7.8	2.7

The percentages of successful devices that passed at various stages of the testing can be seen in Table 2. The top row shows the number of devices with respect to each stage of evaluation. Below row contains the percentage of devices that passed in relation to the total number at that particular stage of evaluation. The ratio of devices from the visual examination stage to passing all tests is 65 %/2.7 %, i.e., 24/1. This type of basic progression is natural for the process of elimination related to evaluating devices. The serpentine and spiral spring structures are more complex and had a greater chance of being fused to the glass substrate or other region of a device. The serpentine actuators yielded over twice the devices when compared to those employing spiral actuators. 3-D accelerometers containing the semi-spiral actuators out-performed the devices employing a spiral structure by 2.9 percent. See Table 1 for the various designs incorporation specific actuators.

## Conclusion

We have described a simple and low-cost testing process for evaluating capacitive accelerometers. The results gathered helped us identify the most reliable designs for future fabrication and testing. This is particularly important when considering the time and costs related to later wire-bonding and dynamic tests. In future fabrications, reliable models could even integrate a piezoelectric material to serve as both a built-in power supply and an on/off switch that responds to changes in motion. Combined with the comb-drive, the resulting device could offer the benefits of being very simple in function, highly sensitive, compact in size, and power efficient. This would be ideal for health and safety monitoring.

The differences in capacitance readings between the anchor-fin regions along the x- and y-planes revealed very small differences in capacitance readings, yet were still relatively consistent in overall performance. The x-directional capacitances offered a larger number of consistently recurring readings in several different percentages while the y-directional performance yielded the highest percentage for a single reading range—approximately 60 %. The readings for the z-plane were the most varied due to the different designs tested that ranged from 1D to 3D areas of sensitivity; a larger surface area between the top and bottom electrodes are another likely reason for the higher degree of variation in readings between these regions. The 3-D functioning devices that passed testing showed relatively reliable performance during these tests. Of these, the semi-serpentine actuators appeared to perform the best during the most recent phase of testing. With a reassessment of the fabrication and testing procedures, the yield should be significantly higher in future evaluations. The z-directional devices provided the highest degree of success in testing, in part due to their simpler function and less testing needed for them. Despite the yield results, the basic testing procedure, itself, is reliable and provides an affordable option to researchers that currently lack funding for complex, automated wafer testing stations. It serves well for evaluating capacitive accelerometers up to the quasi-static level with accurate results.

## Acknowledgments

Authors would like to thank the Lurie Nanofabrication Facility staff at the University of Michigan, Ann Arbor. This research was supported by Early Career Investigator Grant (Grant # C61659) from the Central Michigan University.

## References

- [1] Aswendt, P., Schmidt, C., Zielke, D., & Schubert, S. (2002). HNDT Solution for MEMS Testing on Wafer Level. ZDT.Net.4 (7). Retrieved from <http://www.ndt.net/article/v07n04/aswendt/aswendt.htm>
- [2] Bouchaud, J. (2011). Tablets and Smartphones Spur Record MEMS Revenue Growth in 2011. IHS iSuppli. Retrieved from <http://www.isuppli.com/MEMS-and-Sensors/News/Pages/Tablets-and-Smartphones-Spur-Record-MEMS-Revenue-Growth-in-2011.aspx>.

- [3] Chae, J., Kulah, H., & Najafi, K. (2005). A Monolithic Three-Axis Micro-g Micromachined Silicon Capacitive Accelerometer. *Journal of Microelectronics*, 2(14), 235-242. doi: 10.1109/JMEMS.2004.839347.
- [4] Culhane, K., O'Connor, M., Lyons, D., & Lyons, G. (2005). Accelerometers in Rehabilitation Medicine for Older Adults. *Age and Ageing*, 34, 556-560.
- [5] Demerjian, C. (2011). Memjet Speeds Up Printing with MEMS. Retrieved from <http://semiaccurate.com/2011/02/25/memjet-speeds-up-printing-with-mems>
- [6] Farahani, H., Mills, J., & Cleghorn, W. (2009). Design, Fabrication and Analysis of Micromachined High Sensitivity and 0% Cross-Axis Sensitivity Capacitive Accelerometers. *Microsystem Technology*, 15, 1815-1826.
- [7] Fedder, G. (2003). MEMS Fabrication. *International Test Conference*. Charlotte, NC
- [8] McNulty, J. (2008). A Perspective on the Reliability of MEMS-Based Components for Telecommunications. *SPIE Proceedings*. Paper #6884.
- [9] HP. (2011). HP Seismic Sensor for Oil and Gas Exploration. Retrieved from [http://www.hp.com/hpinfo/newsroom/press\\_kits/2011/sensingsolutions/HP\\_Seismic\\_Sensor\\_wp.pdf](http://www.hp.com/hpinfo/newsroom/press_kits/2011/sensingsolutions/HP_Seismic_Sensor_wp.pdf)
- [10] Whelan, M., Fuchs, M., Gangone, M., & Janoyan, K. (2007). Development of a Wireless Bridge Monitoring System for Condition Assessment Using Hybrid Techniques. *SPIE Proceedings*. Paper #6530. doi: 10.1117/12.715905
- [11] Kaya T and Koser H (2005) A Study of Nonlinear Deflection Dynamics of a Piezoelectric Accelerometer. *COMSOL Multiphysics User's Conference*. Boston, MA.
- [12] Kaya, T., Shiari, B., Petsch, K., & Yates, D. (2011). Design of a MEMS Capacitive Comb-Drive Accelerometer. *COMSOL Multiphysics User's Conference*. Boston, MA.
- [13] O'Sullivan, M., Blake, C., Cunningham, C., Boyle, G., & Finucane, C. (2009). Correlation of Accelerometry with Clinical Balance Tests in Older Fallers and Non-Fallers. *Age and Ageing*, 38, 308-313.
- [14] Man, K.F. (1999). MEMS Reliability for Space Applications by Elimination of Potential Failure Modes through Testing and Analysis. *SPIE, Micromachining and Microfabrication Meeting*. Santa Clara, CA.
- [15] Xu, Z., & Wu, Z. (2008). Sensitivity Analysis of Acceleration-Based Energy Damage Detection Strategy to Load Excitations and Sensor Placement. *Journal of Intelligent Material Systems and Structures*, 20, 413-423. doi: 10.1177/1045389X08095183.
- [16] Lowrie, C., Desmulliez, M., Hoff, L., Elle, O. F., & Fosse, E. (2009). Fabrication of a MEMS Accelerometer to Detect Heart Bypass Surgery Complications. *Sensor Review*, 29(4), 319-325. doi: 10.1108/02602280910986557.
- [17] Petsch, K., & Kaya, T. (2012). Design, Fabrication, and Analysis of MEMS Three-Direction Capacitive Accelerometer. *American Society for Engineering Education North-Central Section Conference*.
- [18] Lemkin, M., & Boser, B. E. (1999). A Three-Axis Micromachined Accelerometer with a CMOS Position-Sense Interface and Digital Offset-Trim Electronics. *IEEE Journal of Solid-State Circuits*, 34(4), 456-468.
- [19] Luo, H., Fedder G., & Carley, L. (2000). A 1 mG Lateral CMOS-MEMS Accelerometer. *IEEE International Conference on Micro Electro Mechanical Systems (MEMS)*. Miyazaki, Japan.

- [20] Maudie, A. H. T., Nielsen, R., Stanerson, D., Bieschke, R., & Miller, M. (2003). MEMS Manufacturing Testing: An Accelerometer Case Study. *International Test Conference*.
- [21] Yurish, S. (2005). Practical Circuits and Interface Techniques for MEMS Accelerometers with Quasi-Digital Output. *Sensors and Transducers Magazine*, 58(8), 352-359.
- [22] Marinkovic, B., Kaya, T., & Koser, H. (2011). Characterization of Ferroelectric Material Properties of Multifunctional Lead Zirconate Titanate for Energy Harvesting Sensor Nodes. *Journal of Applied Physics*, 10, 1-5. doi: 10.1063/1.3524271.
- [23] Liu, Y., Tian, G., Wang, Y., Lin, J., Zhang, Q., & Hofmann, A. H. F. (2008). Active Piezoelectric Energy Harvesting: General Principle and Experimental Demonstration. *Journal of Intelligent Material Systems and Structures*, 20, 575-585. doi: 10.1177/1045389X08098195
- [24] Lee, T., Lee, D. H. Y., Liaw, C. Y. N., Lao, A. I. K., & Hsing, I. (2000). Detailed Characterization of Anodic Bonding Process between Glass and Thin-Film Coated Silicon Substrates. *Sensors and Actuators*, 86, 103-107.
- [25] Schmidt, M. A. (1998, August). Wafer-to-Wafer Bonding for Microstructure Formation. *Proceedings of the IEEE*, 86(8), 1575-1585. doi: 10.1109/5.704262.
- [26] Masson, J., St-Gelais, R., Poulin, A., & Peter, Y. (2010). Tunable Fiber Laser Using a MEMS-Based in Plane Fabry-Pérot Filter. *IEEE Journal of Quantum Electronics*, 46(9), 1313-1319. doi: 10.1109/JQE.2010.2050299
- [27] Miller, S. L., Rodgers, M. S., LaVigne, G., Sniegowski, J. J., Clews, P., Tanner, D. M., & Peterson, K. A. (1998). Failure Modes in Surface Micromachined MicroElectroMechanical Actuators. *IEEE International Reliability Symposium*. Reno, NV. doi: 10.1109/RELPHY.1998.670437.
- [28] Werner, F., & Preston, J. M. (2008). Solutions for Testing MEMS Devices at the Wafer Level. Retrieved from [http://www2.electronicproducts.com/Solutions\\_for\\_testing\\_MEMS\\_devices\\_at\\_the\\_wafer\\_level-article-farcuss\\_jul2008-html.aspx](http://www2.electronicproducts.com/Solutions_for_testing_MEMS_devices_at_the_wafer_level-article-farcuss_jul2008-html.aspx)

## Biographies

THOMAS WHITE is currently a mechanical engineering undergraduate student and a researcher working for Kaya Lab. He has presented his research at several meetings such as ASEE 2013 Midwest Conference in Columbus, Ohio, and at Poster's at the Capital and Student Research and Creative Education Endeavors at Central Michigan University.

KEVIN PETSCH is currently a graduate student at Michigan State University and works at GE. His research focuses on micro electro mechanical systems.

TOLGA KAYA is currently an assistant professor of Electrical Engineering at the School of Engineering and Technology, Central Michigan University. His research includes micro-scale sensor development and bacterial cell manipulation.